Food & Function

Accepted Manuscript

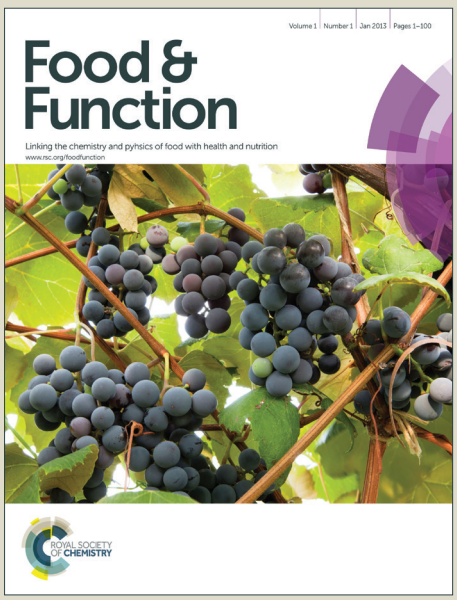

This is an *Accepted Manuscript*, which has been through the Royal Society of Chemistry peer review process and has been accepted for publication.

Accepted Manuscripts are published online shortly after acceptance, before technical editing, formatting and proof reading. Using this free service, authors can make their results available to the community, in citable form, before we publish the edited article. We will replace this *Accepted Manuscript* with the edited and formatted *Advance Article* as soon as it is available.

You can find more information about *Accepted Manuscripts* in the Information for Authors.

Please note that technical editing may introduce minor changes to the text and/or graphics, which may alter content. The journal's standard Terms & Conditions and the Ethical guidelines still apply. In no event shall the Royal Society of Chemistry be held responsible for any errors or omissions in this *Accepted Manuscript* or any consequences arising from the use of any information it contains.

ROYAL SOCIETY OF CHEMISTRY

www.rsc.org/foodfunction

Effect of tannic acid–fish scale gelatin hydrolysate hybride nanoparticles on intestinal barrier function and α-amylase activity

Shao-Jung Wu[1], Yi-Cheng Ho[2], Shun-Zhou Jiang[1], Fwu-Long Mi[3,4*]

1. Department of Chemical Engineering, Ming Chi University of Technology, Taipei 243, Taiwan
2. Department of Bioagriculture Science, National Chiayi University, Chiayi 60004, Taiwan.
3. Department of Biochemistry and Molecular Cell Biology, School of medicine, Taipei Medical University, Taipei 110, Taiwan
4. Graduate Institute of Medical Sciences, College of medicine, Taipei Medical University, Taipei 110, Taiwan

[*]Correspondence to:
Fwu-Long Mi, PhD
Professor
Department of Biochemistry and Molecular Cell Biology
School of medicine
Taipei Medical University
Taipei City, Taiwan 110
Fax: 886-2-2735-6689
E-mail: flmi530326@tmu.edu.tw

Abstract

Practical application of tannic acid is limited because tannic acid readily bind proteins to form insoluble aggregates. In this study, tannic acid was self-assembled with fish scale gelatin hydrolysates (FSGH) to form stable colloidal complex nanoparticles. The nanoparticles prepared from 4mg/ml tannic acid and 4 mg/ml FSGH had a mean particle sizes of 260.8±3.6 nm, and showed a poitive zeta potential (20.4±0.4 mV). The nanoparticles acted as an effective nano-biochelator and free radical scavenger because it provided a large number of adsorption sites for interacting with heavy metal ions and scavenging free radicals. The maximum adsorption capacity for Cu^{2+} ions was 123.5 mg/g and EC_{50} of DPPH radical scavenging activity was 21.6±1.2 μg/ml. Hydroxyl radicals scavenging effects of the nanoparticles were investigated by electron spin resonance spectroscopy. The copper-chelating capacity and free radicals scavenging activity of the nanoparticles were associated with its capacity to inhibit Cu^{2+} ions-induced barrier impairment and hyperpermeability of Caco-2 intestinal epithelial tight junction (TJ). However, α-amylase inhibitory activity of the nanoparticles was significantly lower than that of free tannic acid. The results suggest that the nanoparticles can ameliorate Cu^{2+} ions induced intestinal epithelial TJ dysfunction without severely inhibiting the activity of the digestive enzyme.

Keywords: tannic acid, fish gelatin, nanoparticles, biochelator, antioxidant, tight junction

Introduction

Heavy metals can be accumulated in plants and fish, and are ingested by human populations through the food chain. They were transported through the intestinal mucosa which is the normal route of entry into the body and also the first target for its toxicity. Tight junctions (TJ) create a paracellular barrier in intestinal epithelial cells that modulate selectivity to the permeability of the small intestine. Those metal ions alter tight junction permeability in intestinal monolayer because the toxic properties can affect and impair intestinal epithelial functions.[1] Impairment of tight junction proteins can lead to influx of bacterial endotoxin and result in unwanted immune reactions and systemic inflammation. It has been reported that several naturally occurring compounds exhibit promotive and protective effects on intestinal TJ barrier functions.[2–4]

Tannins are a group of secondary plant metabolites, including hydrolizable, condensed and complex tannic acid, which can be obtained from various plants such as grapes, tea leaves, beans, vegetables, apples, berries, and oak. Tannic acid exhibits several physiological properties such as antioxidant, anti-inflammatory and antimicrobial effects.[5,6] Those health improving and antimicrobial characteristics make this compound a very interesting raw material for biological, medical and food applications.[7] Especially, tannic acid containing abundant adjacent phenolic hydroxyls exhibit excellent binding capacity towards heavy metal ions.[8] However, practical application of tannic acid as an antioxidant and chelating agent in the gastrointestinal tract is limited because it can bind protein in foods in a nonspecific way to form insoluble precipitates and aggregates.[9] Moreover, tannic acid can inhibit the activities of digestive enzymes.[10]

Fish scale is a major fish processing waste which is very rich in collagen.[11] The nutritional values of fish scale collagen are low because they are majorly composed of nonessential amino acids including glycine (Gly), proline (Pro) and hydroxyproline (Hyp).[12] Nevertheless,

enzymatic hydrolyzed collagens from the skin or scales of various fishes, usually called fish gelatin hydrolysate, have been reported to possess some benefit properties, such as free-radical scavenging activity.[13–17]

Incorporation of bioactive flavonoids in nanoparticles can improve the stability, activty and oral bioavailability of the naturally occurring compounds.[18-24] The study aims to develop natural products based nanoparticles to act as effective nano-biochelators and free radical scavengers because the functional nanoparticles can provide a large number of adsorption sites for interacting with heavy metal ions and scavenging toxic free radicals. An easy and mild method was developed in this work to prepare stable colloidal nanoparticles based on tannic acid and fish scale gelatin hydrolysate (FSGH). We found that FSGH had high binding affinity to tannic acid and could form stable colloidal nanoparticles in aqueous solution. The interactions between tannic acid and FSGH, and the chemical and physical properties of tannic acid/FSGH nanoparticles were all characterized. The effect of the nanoparticles on the digestive enzyme activity was compared with their free tannic acid counterpart. Moreover, the protective effect of the nanoparticles on the alterations of epithelia integrity induced by copper(II) ions was investigated using Caco-2 cell monolayers as an in vitro model.

Materials and methods

Materials

FSGH with an average molecular weight less than 3.0 KD was kindly gifted from Challenge Bioproducts Co., Ltd, Taiwan. Tannic acid (Mw 1.7kD), 5,5-Dimethyl-1-pyrroline N-oxide (DMPO), and propidium iodide (PI) were purchased from Sigma–Aldrich Co., Ltd. Copper(II) sulfate pentahydrate and nickel(II) sulfate hexahydrate were obtained from Showa Chemical Industry Co., Ltd (Janpan) and used without further purification.

Amino acid analysis

The FSGH samples were hydrolyzed with 6 M HCl containing 1% phenol (v/v). The working temperature was kept at 110 °C while the reaction continued for 24 h. The digested products were analyzed with an amino acid analyzer (Hitachi L-8900, Japan). Qualitative and quantitative analysis was performed by comparing the amino acid products with the standard amino acids and calculating the area under the peak of each product in chromatography.

Preparation of self-assembled tannic acid/FSGH complex nanoparticles

An amount of FSGH (0.4 g) was dissolved in 100 ml of deionized (DI) water to prepare 4.0 mg/ml FSGH solution. The FSGH solution was flush mixed with different concentrations (2.0, 4.0, 6.0, 8.0 mg/ml) of tannic acid aqueous solutions and the tannic acid/FSGH colloidal nanoparticles formed spontaneously. The suspensions of nanoparticles were continuously stirred for 10 min at 25 °C. A Malvern 3000HS Zetasizer was used to determine the particle sizes and zeta potentials of the nanoparticle suspensions. A drop of the suspensions was placed onto carbon-coated copper grid. Subsequent to deposition for 2 min, surface water on the grid was removed by tapping the grid with a filter paper. The morphology of each sample was characterized by transmission electron microscopy (TEM, Hitachi H-600). To determine the tannic acid loading content, the tannic acid/FSGH complex nanoparticles were centrifuged and the supernatant were quantitatively determined by measuring the absorbance at 275 nm using various concentrations of tannic acid (10-50 ppm) as standards for tannic acid loading assay. The nanoparticles prepared from a tannic acid-to-FSGH weight ratio of 4 mg/4 mg were used for the following analyses.

Characterization of tannic acid and FSGH interactions

Tannic acid, FSGH and tannic acid/FSGH complex nanoparticles were respectively mixed with KBr and the mixtures were pressed into disks for measurement. FTIR spectra were recorded on a Perkin Elmer RX1 Fourier transform infrared (FTIR) spectroscopy in the wavenumber region

between 4000 and 500 cm^{-1}. X-ray diffraction (XRD) data of tannic acid, FSGH and tannic acid/FSGH complex nanoparticles were collected on an X-ray diffractometer (PANalytical, model X'pert pro system). The scan was performed using a monochromatized X-ray beam with Cu Kα radiation (λ = 0.154 nm) to collect 2θ data from 4-50°. Calorimetric measurements were accomplished by a differential scanning calorimetry (DSC), using a DSC TA 2010 (TA Instruments, USA). Precisely weighed tannic acid, FSGH and tannic acid/FSGH complex nanoparticles (3–5 mg) were sealed in aluminium pans and heated at a rate of 10 °C/min from 0°C to 200 °C under an inert atmosphere (10 ml min^{-1} of nitrogen), after performing the calibration with an indium standard. Tannic acid/FSGH complex nanoparticles were added into 400 ppm Cu(II) or Ni(II) ion solutions. After 24 h of adsorption, the tannic acid/FSGH/Ni^{2+} and tannic acid/FSGH/Cu^{2+} complexes were centrifuged and washed with deionized water. Dried tannic acid/FSGH/Ni^{2+} and tannic acid/FSGH/Cu^{2+} complexes analyzed first by XRD according to the abovementioned process.

Heavy metal removal

An amount of $CuSO_4 \cdot 5H_2O$ was dissolved in DI water to prepare the stock solution (1000 mg/L). Tannic acid/FSGH complex nanoparticles (0.2 g) were added in 1000-mL conical flasks containing 500 ml Cu(II) ion solutions (25–400 mg/L, dilution of the stock solution). The mixture was shaken at 100rpm. Adsorption capacities with respect to changes in adsorption temperature were investigated in a temperature range between 30 and 60°C. At predetermined time intervals, the concentrations of metal ions were measured by a PerkinElmer Optima 200DV ICP-OES. The amount of metal ions adsorbed onto the nanoparticles was calculated by:

$$Q = [(C_o - C_t) \times V]/W$$

where Q (mg/g) is the adsorption capacity of metal ions on the nanoparticles, C_o (mg/L) is the initial concentrations of metal ions used in the experiment, C_t (mg/L) is the measured

concentrations of metal ions at time t, V and W are the volume of metal ion solutions (L) and the weight of dry sorbent (g) (tannic acid/FSGH complex nanoparticles), respectively. X-ray diffraction (XRD) data of the

DPPH· radical scavenging assay

The reduction and decolorization of the free radical DPPH· were determined by the previous method.[25] DPPH· was dissolved in methanol (60 μM) with an absorbance value of 0.7 at 517 nm. The tannin/FSGH complex nanoparticles were mixed with deionized water and were serially diluted. An aliquot (3.9 ml) of a 100 mM DPPH· was mixed with 0.1 ml of the diluted nanoparticle samples, making a further 40-fold dilution. The mixtures were incubated in the dark at room temperature for 10 min. A Hitachi U-1900 UV-Vis spectrophotometer was used to measure the decreas of DPPH· concentration at 516 nm. The scavenging ratio for DPPH· radical is calculated as follow:

Scavenging ratio for DPPH· radical (%) = $(1\text{-}Abs_{test\ sample}/Abs_{blank}) \times 100$

Electron spin resonance (ESR) analysis

ESR spectrometry was used to measure hydroxyl radical (OH·) scavenging capacities of the nanoparticles. Fenton-reaction mixture was used to generate hydroxyl radical while DMPO was used to trap the radical. The mixture contained 20 μL of $FeSO_4$ (500 μM)/EDTA (500 μM) mixture, 10 μL of 200 μM H_2O_2, 10 μL of 2 M DMPO, and 30 μL of free tannic acid or nanocomplex. Free tannic acid (50 μg/ml) or complex nanoparticles (50 μg tannic acid equivalent/ml) was added in the Fenton reagent mixture as a final concantration. ESR spin trapping experiments were performed at ambient temperature by an ESR spectrometer (EMX-6/1, Bruker, Karlsruhe, Germany) in a magnetic field of 3482 Gauss (G) with a field modulation amplitude of 2G at X-band (100kHz).

TEER measurements

Caco-2 cells were cultured and grown into monolayers on polycarbonate membrane transwell inserts (Corning Costar Corp., NY). After 3 weeks, the tightness of Caco-2 monolayer was evaluated by measurement of transepithelial electrical resistance (TEER larger than 800 Ω cm^2) using a Millipore Millicell®-ERS meter after pre-equilibrated with Hanks' balanced salt solution (HBSS) buffer. Evaluation the effects of Cu(II) ions on the opening of epithelial tight junctions (TJs) was investigated in Caco-2 cell monolayers in HBSS buffer (Sigma–Aldrich Co., Ltd) with or without the addition of 30 μM $CuCl_2$.[1] Additionally, tannic acid (100 μg/ml) or test nanoparticles (100 μg tannic acid equivalent/ml) was added to the donor compartment, respectively. The change of TEER for the tightness of cell monolayers was measured with a Millicell®-Electrical Resistance System (Millipore Corp., Bedford, MA) to evaluate their protection efficiency.

Fluorescein isothiocyanate–dextran (Mw 4000, Sigma–Aldrich Co., Ltd) was used as a fluorescent probe to study cell permeability. Transport of FITC-dextran (25 μg/ml in the apical compartment) across Caco-2 cell monolayer was quantitatively analyzed by measuring fluorescence intensity in the receiver compartment at different time periods. The intensity of fluorescence emission (FL intensity) was determined by a microplate reader (Victor X, PerkinElmer, USA), with excitation and emission wavelengths set to 488 and 519 nm, respectively. Amount of transported FITC-dextran was calculated using calibration curve of FITC-dextran. The apparent permeability coefficients (Papp) were determined as following:

$$Papp\ (cm/s) = (\triangle Q/\triangle t)/(A \times C_0)$$

where $\triangle Q/\triangle t$ (μg/s) is the cumulative amount transported, A is the diffusion area (1.12 cm^2), and C_0 is the initial FITC-dextran concentration in the donor side (μg/ml).

CLSM visualization of tight junction protein

Caco-2 cell monolayers were incubated with Cu(II) ions (30 μM) and tannic acid (100 μg/ml) or

nanoparticles (100 μg tannic acid equivalent/ml). After 120 min, cells were fixed in paraldehyde, permeabilized with 0.2% Triton X-100, and treated with RNase (100 μg/ml) after removal of Cu(II) ions, tannic acid and test nanoparticles. A normal goat serum was used to block the cells (Jackson ImmunoResearch Laboratories, West Grove, PA). The cells were incubated with rabbit anti-ZO-1 monoclonal antibody (Zymed Laboraties) and subsequently stained by a Cy-3 conjugated goat anti-rabbit IgG (Jackson ImmunoResearch Laboratories). Dislocation of ZO-1 protein in Caco-2 cells was examined under a confocal laser scanning microscopy (CLSM, Leica TCS SP2).

Inhibition of α-amylase activity

Experiments on the inactivation of α-amylase by tannic acid or tannic acid/FSGH complex nanoparticles were carried out using the method according to the literature.[10] A reaction mixture of starch solution (1%) and α-amylase solution (1–5 U/ml) was incubated at 37 °C and was subsequently assayed by measuring the absorbance at 540 nm. The α-amylase inhibitory assay was measured using starch as a substrate (1.0 w/v) with or without containing tannic acid (0.5 mg/ml) or nanoparticles (0.5 mg tannic acid eq./ml). Lineweaver–Burk (LB) analysis was performed by measuring the inhibition at different concentrations of starch (0.5, 0.75, 1.0, 1.5, 2.0 and 5.0% w/v). The data were fitted to the Michaelis-Menten equation using LB plot to analyze the inhibition mode.

Statistical analyses

All measurements were replicated three times and data were expressed as the mean±standard deviation. Statistical analysis was performed with the analysis of variance (ANOVA) procedure using SAS version 9.1 (SAS Institute, Cary, NC, USA). The differences among the experimental data were determined using Duncan's multiple range tests with significance level at $P<0.05$.

Results and discussion

Amino acid compositions

The amino acid composition of FSGH shown in Table 1 was expressed as units for amino acids (% of total amino acid residues). Because FSGH is hydrolyzed collagen-derived small peptides, glycine (Gly) is the most abundant amino acid (335.87/1000) in the polypeptide. The second and third abundant amino acids in FSGH are proline (125.60/1000) and hydroxyproline (89.35/1000), which play important roles in the interaction of tannic acid with FSGH.

Characterization of tannic acid/FSGH colloidal complex

In this study, the colloidal complex nanoparticles were spontaneously formed by adding tannic acid into the FSGH solution, indicating the presence of specific interactions between tannic acid and FSGH. The chemical structures of tannic acid, FSGH and tannic acid/FSGH complex nanoparticles were characterized by FT-IR spectra. Tannic acid demonstrated absorption bands at around 1713 cm^{-1} and 1609 cm^{-1} due to the vibration of ester and benzene ring. FSGH demonstrated characteristic absorptions of C=O stretch (amide I, 1657 cm^{-1}) and N–H stretch (amide II, 1541 cm^{-1}) (Fig. 1A). The large bands at around 1331 cm^{-1} and 1202 cm^{-1} were assigned to the vibrations of $–CH_3$ symmetrical deformation and O–H deformation. Other characteristic peaks at 3100–3400 cm^{-1} and 2850–3000 cm^{-1} were assigned to O–H stretch of tannic acid (hydroxyl groups bonded to the aromatic ring) and C–H stretch of FSGH. The intensity of the characteristic absorptions of ester (1713 cm^{-1}, C=O stretch) in tannic acid decreased while the absorption band of benzene ring shifted from 1608 cm^{-1} to 1616 cm^{-1} after the formation of tannic acid/FSGH complex nanoparticles. Moreover, the amide II absorption band (N–H stretch) in FSGH shifted from 1541 cm^{-1} to 1536 cm^{-1}. The results indicated that the existence of interspecific interactions between tannic acid and FSGH. The formation of colloidal tannic acid/FSGH nanoparticles may be associated with hydrogen bonding between the

hydroxyl groups in tannic acid and the hydroxyproline residues in FSGH or even by π–π stacking interactions between the benzene rings in tannic acid and the aromatic amino acids in FSGH.[26]

Fig. 1B shows the DSC analysis of FSGH, tannic acid and tannic acid/FSGH complex nanoparticles (TA/FSGH NPs). FSGH and tannic acid demonstrated endothermic peaks at 132.2 °C and 123.7 °C, respectively. The endothermic transitions of FSGH and tannic acid occurred from the loss of bound water which was corresponding to the moisture content and water evaporation. This peak disappeared due to the displacement of bound water from the binding sites through the formation of tannic acid/FSGH complex nanoparticles. A new endothermic transition appeared at a lower temperature (76.5 °C) because tannic acid creates new interchain hydrogen bonding in FSGH. This interaction was also accompanied with the hydrophobic interactions between the benzene ring in tannic acid and the hydrophobic amino acid residues in the polypeptides.[26] After the adsorption of metal ions, the temperature of endothermic transition increased to 88.4 °C (Cu^{2+} ions) and 105.7 °C (Ni^{2+} ions), and the peaks became sharper owing to the formation of metal complexes. Fig. 1C shows the photographs of colloidal solutions of tannic acid/FSGH nanoparticles. The tannic acid and FSGH solutions were both clear. However, the solutions turned milk-white after adding FSGH into tannic acid solutions because of the formation of colloidal complex nanoparticles. Visualization of the photographs indicated that the turbidity of colloidal solutions increased with increasing the concentrations of tannic acid. TEM imagine confirms the spherical shape of the nanoparticles prepared from 4 mg/ml tannic acid and 4 mg/ml FSGH (tannic acid-to-FSGH weight ratio = 4 mg/4 mg) (Fig. 1D). However, the nanoparticles prepared from 8 mg/ml tannic acid and 4 mg/ml FSGH (tannic acid-to-FSGH weight ratio = 8 mg/4 mg) was slightly aggregated. Therefore, the nanoparticles prepared from a tannic acid-to-FSGH weight ratio of 4 mg/4 mg were used for the following analyses because of

their high stability and dispersibility in water.

Properties of self-assembled tannic acid/FSGH colloidal complex nanoparticles

Particle sizes and surface charges of the complex nanoparticles were affected by tannic acid-to-FSGH ratio. By keeping FSGH concentration at 4 mg/ml, the nanoparticles prepared at low tannic acid concentrations (2 mg/ml) were small and the average particle size was 190.5±2.9 nm (Table 2). In contrast, the particle size increased to larger than 500 nm when tannic acid concentration increased to 8 mg/ml. The results suggest that the complex nanoparticles start to aggregate at high tannic acid concentrations. Accordingly, the tannic acid concentration plays an important role to affect the stability of prepared complex nanoparticles.

The zeta potentials of complex nanoparticles linearly decreased with the increase of tannic acid concentrations. It is known that tannic acid is an ester formed by the condensation of gallic acid, which contains phenolic hydroxyls on the aromatic rings. The phenolic hydroxyls (Ar–OH) can be deprotonated in aqueous solutions to form phenoxide anions ($Ar–O^-$). In contrast, FSGH has an average isoelectric point similar to type A gelatin (pI = 7.0–9.0). As shown in Table 2, the positive zeta potentials were observed for the complex nanoparticles, revealing that a positively charged FSGH layer was closely attached to the surface of nanoparticles, which ensured the colloidal stabilization. As shown in Table 2, the tannic acid loading content increases with the increase of tannic acid concentration.

Adsorption of heavy metals

Fig. 2A shows the X-ray diffractograms (XRD) for tannic acid, FSGH and tannic acid/FSGH complex nanoparticles. As can be seen, tannic acid and FSGH respectively show diffraction peaks at 2θ = 24.9° and 20.8°. XRD results showed a new diffraction peak around 22.5° because the collagen-like, triple-helical structure was renatured in FSGH. The diffractograms of Cu^{2+}-binding nanocomplexes (tannic acid/FSGH/Cu^{2+}) demonstrated strong, characteristic

diffraction peaks of copper complexes at 18.1° and 25.9°, and Ni^{2+}-binding nanocomplexes (tannic acid/FSGH/Ni^{2+}) at 20.1°, 22.9° and 30.6°. Fish gelatin is a poor metal-chelating ligand showing low affinity for metal ions. However, after hydrolysis, the metal-chelating ability of FSGH can be improved due to the formation of more electron-donating, carboxyl and amino groups.[27] The high electrophilicity of the pyrogallol ring in tannic acid has high affinity to several heavy metal ions, while the galloyl groups can improve the reaction ability of tannic acid with metal ions.[28] As shown in Fig. 1B, Cu^{2+} and Ni^{2+} ions stabilized FSGH by shifting the endothermic transitions to slightly higher temperatures (from 76.5 °C to 88.4 °C and 106.7 °C) because the lone electron pairs of the amine and carboxylic acid in FSGH were donated into d orbitals of those transition metal ions to form coordinate covalent bonds. The result reveals that tannic acid/FSGH complex nanoparticles may act as a potent biosorbent for removing hazardous metal ions.

Copper ions catalyze the production of reactive oxygen species (ROS) via Fenton and Haber–Weiss reactions. Cu^{2+} ions can be reduced by intracellular glutathione (GSH) to catalyze the conversion of H_2O_2 to hydroxyl radicals.[29] Cu^{2+} ions can also act as electron acceptors which show high affinity to lone pair electrons on the phenolic hydroxyls of tannic acid. Therefore, Cu^{2+} was selected for the examination of the isothermal and kinetic adsorption properties of tannic acid/FSGH complex nanoparticles. The pyrogallol or galloyl groups in tannic acids binds metal ions at high affinity as the phenolic hydroxyls were deprotonated.[28] Tannic acid with two or three charged phenolic hydroxyl groups adjacent to each other, is an effective bidentate ligand capable of forming a five-membered ring chelate complex of Cu(II) ion. Langmuir isotherms can be used to evaluate the equilibrium adsorption of Cu(II) ion on tannic acid/FSGH complex nanoparticles.[30] The adsorption capacity increased with increasing the equilibrium concentration of Cu^{2+} ions. The expression for the Langmuir isotherm is

$$Q_e = \frac{Q_m K_L C_e}{1+K_L C_e}$$

where Q_e and C_e are the adsorption capacity (mg/g) and the concentration of Cu(II) ions at equilibrium (mg/L). $(1/Q_e)$ is plotted against $(1/C_e)$ to calculate Q_m, the monolayer adsorption capacity of Cu(II) ions (mg/g), and K_L (L/mg) (Fig. 2B). The Langmuir isotherm model considers the adsorbent surface as homogeneous and can provide identical sites for a single molecular layer adsorption. Maximum adsorption occurs subsequent to the formation of a monolayer of saturated solute (Cu^{2+} ions) on the surface of the nanoparticles. The maximum adsorption values estimated from the equation for Cu^{2+} ions was 123.5 mg/g (Table 3), suggesting that the nanoparticles were efficient in adsorbing Cu^{2+} ions.

The kinetics of uptake of Cu^{2+} ions by nanoparticles was determined with respect to pseudo-second-order kinetic model shown as the follows:[31]

$$t/Q_t = 1/k\, Q_e^2 + t/Q_e$$

where Q_e (mg/g) and Q_t (mg/L) are the amount of adsorbed Cu^{2+} (mg/g) at equilibrium and at time, t. The *k* is the pseudo-second-order rate constant (min^{-1}). The rate constants *k* and the correlation coefficient (R^2) were determined by linear plots of t/Q_t vs. *t* (Fig. 2C). Table 3 summarizes adsorption kinetic parameters. The straight line plots of pseudo-second-order kinetic models acquires correlation coefficients of 0.9975 for the adsorption of Cu^{2+} ions, suggesting that pseudo-second-order equation is a suitable model to describe the kinetic adsorption. Chemisorption involving the electron donor-acceptor couple between the nanoparticles and metal ions became the rate-limiting step in the adsorption process.

Energies and entropy (Δ G°, Δ H°, and Δ S°) are useful thermodynamic parameters which can be employed to determine the energy change and spontaneity of an adsorption process. The apparent equilibrium constant (K_c) of the adsorption was calculated as follow:[31]

$K_c = X_e/(C_i - X_e)$

where X_e and C_i are the adsorbed and initial concentration of Cu^{2+} ions (mg/L). The relationship between the Gibbs free energy change (ΔG^o) and K_C is temperature dependent and was allowed to calculate ΔH^o and ΔS^o by using the following relationships:

$$\Delta G^o = -RT\ln K_C$$

$$\ln K_c = -\frac{\Delta H^o}{RT} + \frac{\Delta S^o}{R}$$

where R (8.314 J/mol K) is the gas constant and T is the absolute temperature (K). The values of ΔH^o and ΔS^o calculated from a linear plot of $\ln K_c$ vs. 1/T are shown in Table 3. The adsorption process was endothermic and spontaneous according to the positive signs of ΔH^o and the negative signs of ΔG^o. The ΔG^o values decreased with increasing the temperature, suggesting that high temperatures are of benefit to adsorption. The irregularly increased randomness in the nanoparticles-metal ion interaction is confirmed by the positive values of ΔS^o.

Electron spin resonance (ESR)

Plant polyphenols was known to possess potent free radical scavenging activity. Tannic acid, a polymeric polyphenolic compound, is a more powerful free radical scavenger than its monomeric phenolic counterparts, due to the propinquity of aromatic hydroxyl groups in the condensed tannic acid.[32] The tannin equivalent required to scavenge 50% of initial DPPH· radical by the complex nanoprticles was expressed as EC_{50}. The EC_{50} values were reduced as the tannin-to-FSGH ratios in the nanoprticles increased (Table 2). The results shows that the tannin/FSGH nanoprticles prepared with larger tannin-to-FSGH ratios has considerable antioxidant powers in scavenging DPPH·radical as indicated by the lower EC_{50} values.

It is known that reduced glutathione (GSH) catalyzes the redox cycling of exogenous/endogenous copper ions to produce superoxide anion ($O_2\cdot^-$). The free radical isn't

stable and quickly decomposes to hydroxyl radicals (OH·).[29] As shown in Fig. 2D, ESR spectra of hydroxyl radical, produced from Fenton-reaction reagents and DMPO, consisted of a 1:2:2:1 quartet signal amplitude of DMPO-OH (a_N = 1.50 mT, a_H = 1.50 mT). The OH· scavenging capacity of free tannic acid, FSGH, and the complex nanoparticles, were investigated by ESR analysis. The additions of free tannic acid (50 μg/ml) or tannic acid/FSGH complex nanoparticles (50 μg tannic acid equivalent/ml) to the mixture efficiently decreased the intensity of the DMPO-OH spin adduct signal. The OH· scavenging ratios of the nanoparticles were estimated from the signal-intensity ratio of the sample to the control. The free tannic acid had high OH· scavenging activity, showing a OH· scavenging ratio of 47.2%. However, at the same tannic acid equivalent, the OH· scavenging ratio of the nanoparticles was 1.2 folds (56.6%) higher than its free tannic acid counterpart.

The results suggested that both free tannic acid and tannic acid/FSGH complex nanoparticles showed powerful OH· scavenging activities. As shown in this figure, free tannic acid is a stronger OH· scavenger than that of FSGH, indicating that different components of the nanoparticles (tannic acid and FSGH) may differ in their OH· scavenging activity. However, the OH· scavenging ratio of the nanoparticles was higher than that of free tannic acid at the same tannic acid equivalent due to the assistance of FSGH. Although the free radical scavenging activity of FSGH was less than that of tannic acid, FSGH has a tendency to inhibit the generation of OH. Therefore, the combination of tannic acid and FSGH in nanoparticles enhanced the OH· scavenging activity. It was assumed that the hydroxyl radical could be quenched by the nanoparticles through metal ion chelation. This assumption was confirmed by high Cu^{2+} chelating capacity of the nanoparticles (Table 3). Furthermore, the hydroxyl radical scavenging activity of the nanoparticles may also attributed to their superior free radical scavenging capability (Table 2). The results suggested that the nanoparticles inhibited the

generation of OH· by two actions, including direct scavenging of OH· and chelation with Cu^{2+} ions.

Tight junction permeability

Heavy metal ions can interact with cell membrane, inducing the generation of intracellular ROS and tight junction dysfunction.[33] Some polyphenols were reported to protect the epithelial barrier function of Caco-2 Cells.[34] Measurements of TEER in Caco-2 cell monolayers were shown in Fig. 3A. By treating Caco-2 cell with 30 μM Cu^{2+} ions for 2 h, the TEER value dcreased to 47.3±4.2% of its initial value. Tannic acid (100 μg/ml) effectively inhibited tight-junction opening induced by Cu^{2+} ions. The TEER value slightly dereased to 71.4±5.2% of initial value. However, the inhibition efficiency of complex nanoparticles against Cu^{2+}-induced tight junction opening decreased with increasing the time of treatment. After 2h of treatment, the TEER value of the nanoparticle-protected group (100 μg/ml tannic acid equivalent/ml) was similar to that of the non-protected group (53.4±6.3% vs 47.3±4.2% of the initial values). Tannic acid is a water soluble compound which reacts immediately with Cu^{2+} ions to form tannic acid/Cu^{2+} complex. In contrast, adsorption of Cu^{2+} into tannic acid/FSGH nanoparticle is time-dependent. As shown in Fig. 2C, adsorption of Cu^{2+} by nanoparticles follows a pseudo-first-order kinetic model. This result suggests that that adsorption of Cu^{2+} ions by the nanoparticles was not as faster as free tannic acid. The TEER value reversibly increased after removing exogenous Cu^{2+} ions, indicating that the removal of copper ions was able to induce a reversible increase in tight junction permeability (Fig. 3B). After 2400 minutes of recovery, the TEER values of Caco-2 cell treated with Cu^{2+} ions in the presencec of either tannic acid or tannic acid/FSGH nanoparticles were 91.8±2.5% and 82.4±3.6% of their initial values while those without containing nanoparticles only recovered to 75.1±3.2% of their initial values.

The transepithelial permeability of Caco-2 cell monolayers were also determined by

measuring paracellular flux of fluorescein isothiocyanate (FITC) labeled dextrans (FITC-dextran). The permeability coefficient (Papp) of macromolecular FITC-dextran increased by adding 30 μM Cu^{2+} ions to Caco-2 monolayer (Fig. 3C). The increases in FITC-dextran permeability was corresponding to the increases in opening of tight-junction as indiated by the TEER analysis. Dextran is a macromolecule which gains access through the tight junctions only when TEER decreases below a certain value. However, as Caco-2 cells monolayer was co-treated with Cu^{2+} ions and tannic acid, the amount of FITC-dextran transported through Caco-2 cells was considerably reduced. These results implied that the complex nanoparticles can be used as a biochelator to reduce the effects of Cu^{2+} ions on the tight junction barrier impairment and paracellular transport of macromolecules. The protective effects may be attributed to its copper-chelating capacity and free radicals scavenging activity therefore reduced oxidative stress in Caco-2 cells.

Confocal laser-scanning microscopy (CLSM) was carried out to investigate the tight junction protein, ZO-1, in Cu^{2+}-treated Caco-2 cells. The fluorescent images of ZO-1 in Caco-2 cells after 2 h of incubation with Cu^{2+} ions (30 μM) were shown in Fig. 3D. The green fluorescence indicated ZO-1 protein whereas the red fluorescence indicated nuclei. Localization of the tight junction protein, ZO-1, wasn't affected by treatment with Cu^{2+} ions, in either the presence or absence of nanoparticles (100 μg/ml tannic acid equivalent/ml). The result indicated that changes in the tight-junction tightness weren't associated with the localization of the junctional protein.

Inhibition of α-amylase activity

Polyphenols can interact with digestive enzymes and has a negative effect on intestinal digestion of protein and starch, consequently reduces the nutritional value of foods.[35] Tannic acid inhibited the activity of α-amylase in a dose-dependent way. It was reported that tannic acid is a

reversible inhibitor can bind to α-amylase through weak non-covalent interactions including hydrophobic interactions and hyrogen bonds.[10] As shown in Fig. 4A, α-amylase inhibitiory activities were measured at different concentrations of tannic acid. The inhibition ratio increases linearly with tannic acid concentration up to 80%. The extent of inhibition of α-amylase by nanoparticles was much lower than than free tannic acid at the same concentrations. The IC_{50} values (inhibition of 50% enzyme activity) indicated that α-amylase inhibitory activity of nanoparticles (1.94 mg/ml) was about 6.3-fold less than that of free tannic acid (0.31 mg/ml).

Fig. 4B shows a Lineweaver-Burk plot of the reciprocal of reaction rate (1/V) vs. the substrate concentration (1/[S]). The maximum velocity (V_{max}) and constant (K_m) were estimated by fitting the Michaelis-Menten equation. The plot lines show that α-amylase was noncompetitively inhibited by tannic acid, suggesting that the binding of tannic acid to the enzyme reduces its activity but does not affect the binding of substrate. This figure also shows the effect of tannic acid/FSGH complexation on inhibition activity of α-amylase. By changing the inhibitor from free tannic acid to complex nanoparticles, the maximum velocity (V_{max}) increased, however, the Michealis–Menten constant (K_m) remained the same. These results indicate that the inhibitions (free tannic acid and complex nanoparticles) were non-competitive patterns. However, the inhibition activity against α-amylase of the complex nanoparticles was significantly lower than that of free tannic acid.

Tannic acid is a noncompetitive inhibitor can bind to digestive enzymes at a different site than the active site specific for the substrate. FSGH has strong binding affinity to tannic acid, consequently rendered its enzyme inhibitory activity after forming nanoparticles. Although the complex nanoparticle has high adsorption capacity for Cu(II) ions and effective free radicls scavenging capability, the enzyme inhibitory activity of the tannic acid/FSGH nanoparticle was significantly reduced as compared to its free tannic acid counterpart. The results reveal that the

456 nano-chelator and radical scavenger may not severely affect the functions of digestive enzymes
457 in the GI tract.

458 ## Conclusions

459 We have developed the nanoparticles containing tannic acid and FSGH, and their
460 physicochemical properties, free radical scavenging activities and Cu^{2+} adsorption capacities
461 were evaluated. The nanoparticle was an effective adsorbent to remove Cu^{2+}, and the maximum
462 adsorption capacity was high (123.5 mg/g). The nanoparticle was efficient in scavenging
463 hydroxyl radicals (OH·) due to a synergistic free radical scavenging activity of tannic acid with
464 FSGH. The nanoparticles showed a potential in ameliorating Cu^{2+} ions induced intestinal
465 epithelial TJ dysfunction without severely inhibiting the activity of the digestive enzyme.
466 Suppression of Cu^{2+} ions induced intestinal epithelial TJ dysfunction and hyperpermeability by
467 the nanoparticles was associated with the free radicals scavenging activity and Cu^{2+}-binding
468 capability.

469 ## Acknowledgments

470 This work was supported by a grant (NSC 100-2221-E-131-013) from the Ministry of Science
471 and Technology, Taiwan, ROC. We would like to express our thanks to Challenge Bioproducts
472 Co., Ltd for the kindly gifted FSGH.

References

1 S. Ferruzza, M. L. Scarino, G. Rotilio, M. R. Ciriolo, P. Santaroni, A. O. Muda and Y. Sambuy, *Am. J. Physiol.*, 1999, **277**, G1138–G1148.

2 H. J. Kim, E. K. Lee, M. H. Park, Y. M. Ha, K. J. Jung, M. S. Kim, M. K. Kim, B. P. Yu and H. Y. Chung, *Phytother. Res.*, 2013, **27**, 362–367.

3 T. Suzuki and H. Hara, *J. Nutr. Biochem.*, 2011, **22**, 401–408.

4 L. L. Gu, N. Li, J. F. Gong, Q. R. Li, W. M. Zhu and J. S. Li, *J. Infect. Dis.*, 2011, **203**, 1602–1612.

5 N. P. Seeram, L. S. Adams, S. M. Henning, Y. T. Niu, Y. J. Zhang, M. G. Nair and D. Heber, *J. Nutr. Biochem.*, 2005, **16**, 360–367.

6 M. R. Gonzalez-Centeno, M. Jourdes, A. Femenia, S. Simal, C. Rossello and P. L. Teissedre, *J. Agric. Food Chem.*, 2013, **61**, 11579–11587

7 H. Akiyama, K. Fujii, O. Yamasaki, T. Oono and K. Iwatsuki, *J. Antimicrob. Chemother.*, 2001, **48**, 487–491.

8 M. Gurung, B. B. Adhikari, S. Morisada, H. Kawakita, K. Ohto, K. Inoue and S. Alam, *Bioresour. Technol.*, 2013, **129**, 108–117.

9 E. Obreque-Slier, C. Mateluna, A. Pena-Neira and R. Lopez-Solis, *J. Agric. Food Chem.*, 2010, **58**, 8375–8379.

10 W. Zhao, V. Iyer, F. P. Flores, E. Donhowe and F. Kong, *Food Funct.*, 2013, **4**, 899–905.

11 W. Yang, B. Gludovatz, E. A. Zimmermann, H. A. Bale, R. O. Ritchie and M. A. Meyers, *Acta. Biomater.*, 2013, **9**, 5876–5889.

12 F. Pati, B. Adhikari and S. Dhara, *Bioresour. Technol.*, 2010, **101**, 3737–3742.

13 T. S. Vo, D. H. Ngo, J. A. Kim, B. Ryu and S. K. Kim, *J. Agric. Food Chem.*, 2011, **59**, 12193–12197.

14 D. H.Ngo, B. Ryu and S. K. Kim, *Food Chem.* **2014**, *143*, 246–255.

15 S. W. Himaya, B. Ryu, D. H. Ngo and S. K. Kim, *J. Agric. Food Chem.*, 2012, **60**, 9112–9119.

16 M. Chalamaiah, B. Dinesh Kumar, R. Hemalatha and T. Jyothirmayi, *Food Chem.*, 2012, **135**, 3020–3038.

17 P. Kittiphattanabawon, S. Benjakul, W. Visessanguan and F. Shahidi, *Food Chem.*, 2012, **135**, 1118–1126.

18 Z. Li, and L. Gu, *J. Agric. Food Chem.*, 2014, **62**, 1301–1309.

19 B. Hu, Y. W. Ting, X. Q. Yang, W. P. Tang, X. X. Zeng and Q. R. Huang, *Chem. Commun*, 2012, **48**, 2421–2423.

20 B. Li, W. Du, J. Jin and Q. Du, *J. Agric. Food Chem.*, 2012, **60**, 3477–3484.

21 J. Xue, C. Tan, X. M. Zhang, B. Feng and S. Q. Xia, *J. Agric. Food Chem.*, 2014, **62**, 4677–4684.

22 Y. Q. Zhang, Y. G. Niu, Y. C. Luo, M. Ge, T. Yang, L. L. Yu and Q. Wang, *Food Chem.*, 2014, **142**, 269–275.

23 Y. C. Chen, S. H. Yu, G. J. Tsai, D. W. Tang, F. L. Mi and Y. P. Peng, *J. Agric. Food Chem.*, 2010, **58**, 6728–6734.

24 D. W. Tang, S. H. Yu, Y. C. Ho, B. Q. Huang, G. J. Tsai, H. Y. Hsieh, H. W. Sung and F. L. Mi, *Food Hydrocolloids***,** 2013, **30**, 33–41.

25 S. H. Yu, H. Y. Hsieh, J. C. Pang, D. W. Tang, C. M. Shih, M. L. Tsai, Y. C. Tsai and F. L. Mi, *Food Hydrocolloids*, 2013, **32**, 9–19.

26 R. Goncalves, N. Mateus, I. Pianet, M. Laguerre and V. de Freitas, *Langmuir*, 2011, **27**, 13122–13129.

27 B. Giménez, A. Alemán, P. Montero and M. C. Gómez-Guillén, *Food Chem.*, 2009, **114**,

976–983.

28 X. Huang and X. Liao, B. Shi, *J. Hazard. Mater.*, 2010, **173**, 33–39.

29 H. Speisky, M. Gomez, C. Carrasco-Pozo, E. Pastene, C. Lopez-Alarcon and C. Olea-Azar, *Bioorg. Med. Chem.*, 2008, **16**, 6568–6574.

30 S. J. Wu, T. H. Liou and F. L. Mi, *Bioresour. Technol.*, 2009, **100**, 4348–4353.

31 S. J. Wu, T. H. Liou, C. H. Yeh, F. L. Mi and T. K. Lin, *J. Appl. Polym. Sci.*, 2013, **127**, 4573–4580.

32 A. E. Hagerman, K. M. Riedl, G. A. Jones, K. N. Sovik, N. T. Ritchard, P. W. Hartzfeld and T. L. Riechel, *J. Agric. Food Chem.*, 1998, **46**, 1887–1892.

33 S. Ferruzza, M. Scacchi, M. L. Scarino and Y. Sambuy, *Toxicol. In Vitro*, 2002, **16**, 399–404.

34 C. Carrasco-Pozo, P. Morales and M. Gotteland, *J. Agric. Food Chem.*, 2013, **61**, 5291–5297.

35 G. Williamson, *Mol. Nutr. Food Res.*, 2013, **57**, 48–57.

535 **Figure Captions**

536 Fig. 1. (A) FTIR analysis of the chemical structures of tannic acid, FSGH, and tannic
537 acid/FSGH complex nanoparticles (TA/FSGH NPs), (B) DSC analysis of tannic acid,
538 FSGH, tannic acid/FSGH complex nanoparticles (TA/FSGH NPs), and their metal
539 complexes (TA/FSGH/Cu^{2+} and TA/FSGH/Ni^{2+} complexes), (C) photographs of
540 colloidal dispersion of tannic acid/FSGH nanoparticles (TA/FSGH NPs), tannic
541 acid-to-FSGH weight ratio = 2/4, 4/4, 6/4, and 8/4 (mg/mg), (D) TEM micrographs of
542 tannic acid/FSCH nanoparticles (TA/FSGH NPs): (a) tannic acid-to-FSCH weight ratio
543 = 4 mg/4 mg), (b) tannic acid-to-FSCH weight ratio = 8 mg/4 mg)

544 Fig. 2. (A) X-ray diffractograms (XRD) for tannic acid, FSGH, tannic acid/FSGH nanoparticles
545 (TA/FSGH NPs), and their metal complexes (TA/FSGH/Cu^{2+} and TA/FSGH/Ni^{2+}
546 complexes), (B) fitting experimental data of Langmuir isotherm for adsorption isotherm,
547 (C) fitting experimental data of the pseudo-second-order model for adsorption kinetic,
548 (D) ESR spectra of the scavenging of hydroxyl radical generated from Fenton-reaction
549 by tannic acid (50 μg/ml), FSGH (50 μg/ml) and TA/FSGH NPs (50 μg/ml tannic acid
550 equivalent).

551 Fig. 3. Effect of Cu^{2+} ions on TEER in Caco-2 cell monolayers. TEER values were measured in
552 untreated cells (control), copper-treated cells (30μM $CuCl_2$), and in copper-treated cells
553 with addition of 100 μg/ml tannic aid (30μM $CuCl_2$/tannic acid) or 100 μg/ml tannic aid
554 equivalent of nanoparticles (50μM $CuCl_2$/TA/FSGH NPs) after 2 h of treatment (A) and
555 24 h of recovery (B); (C) Effect of Cu^{2+} ions on permeability coefficient (Papp) of
556 macromolecular FITC-dextran in untreated cells (control), copper-treated cells (30μM
557 $CuCl_2$), and in copper-treated cells with addition of 100 μg/ml tannic aid (30μM
558 $CuCl_2$/tannic acid) or 100 μg/ml tannic aid equivalent of nanoparticles (30μM

559 $CuCl_2$/TA/FSGH NPs), (D) fluorescent images of ZO-1 in original Caco-2 cells and in
560 the Cu^{2+}-treated cells (after 2 h of incubation).

561 Fig. 4. (A) The inhibition effects of different concentration of tannic acid, FSGH, and tannic
562 acid/FSCH nanoparticles (TA/FSGH NPs) on α-amylase activities, (B)
563 Lineweaver–Burk analysis of inhibition mode in the presence of free tannic acid (0.5
564 mg/ml) and tannic acid/FSCH nanoparticles (TA/FSGH NPs, 0.5 mg tannic acid
565 equivalent/ml).

Table 1. Amino acid composition of FSGH

FSGH	Amino acids g/ 100g protein	Units for amino acids (%)
Aspartic acid	5.17	4.24
Threonine	2.84	2.60
Serine	3.33	3.46
Glutamic acid	10.18	7.54
Glycine	23.14	33.58
Alanine	9.25	11.31
Cysteine	0.62	0.56
Valine	2.60	2.42
Methionine	1.62	1.18
Isoleucine	1.67	1.39
Leucine	3.04	2.53
Tyrosine	0.95	0.57
Phenylalanine	2.23	1.47
Lysine	2.97	2.22
Histidine	1.50	1.05
Arginine	4.63	2.89
Proline	13.26	12.6
Hydroxyproline	10.75	8.94

Table 2. Average size, zeta potential, tannic acid loading content of tannic acid (2-8 mg)/FSGH (4 mg/ml) nanoparticles

Tannic acid (mg/ml)	average size (nm)	zeta potential (mV)	loading content (μg/mg)	DPPH scavenging EC_{50} (μg/ml)
tannic acid/FSGH nanoparticles				
2	190.5±2.9	22.7±0.9	243.3±7.9	34.8±2.6
4	260.8±3.6	20.4±0.4	389.5±8.5	21.6±1.2
6	447.7±5.5	19.7±0.5	469.1±11.4	17.8±0.5
8	627.9±4.8	17.5±0.5	513.6±15.5	16.1±0.6
free tannic acid				14.3±0.8

Table 3. Isotherm and Kinetic constants for adsorption of Cu(II) ion onto tannic acid/FSGH nanoparticles (tannic acid-to-FSGH weight ratio = 4 mg/4 mg).

model	Cu(II) ion
Langmuir isotherm	
Q_m (mg/g)	123.45
K_L (L/mg)	0.0162
R^2	0.9996
Kinetic model	
Q_e(exp.)(mg/g)	24.37
Pseudo-second order constant	
K (min^{-1})	4.5×10^{-3}
Q_e(theor.)(mg/g)	24.51
R^2	0.9975
Thermodynamic parameters	
ΔG^o (J/mol)	
30°C	-979.26
35°C	-1199.1
40°C	-1249.6
ΔH^o (KJ/mol)	15.56
ΔS^o (J/mol)	48.31

Graphic Abstract

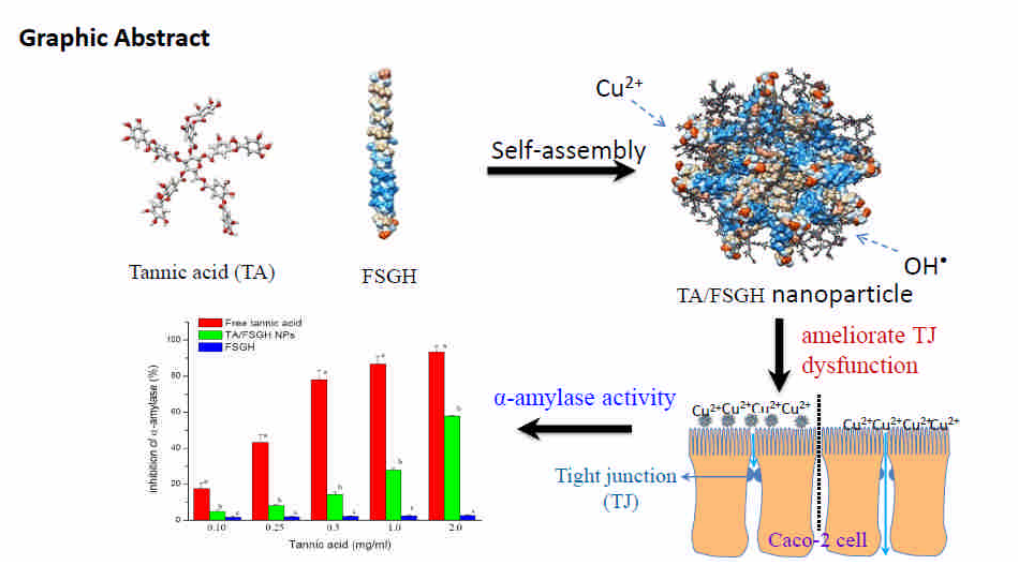

624

Fig. 1A

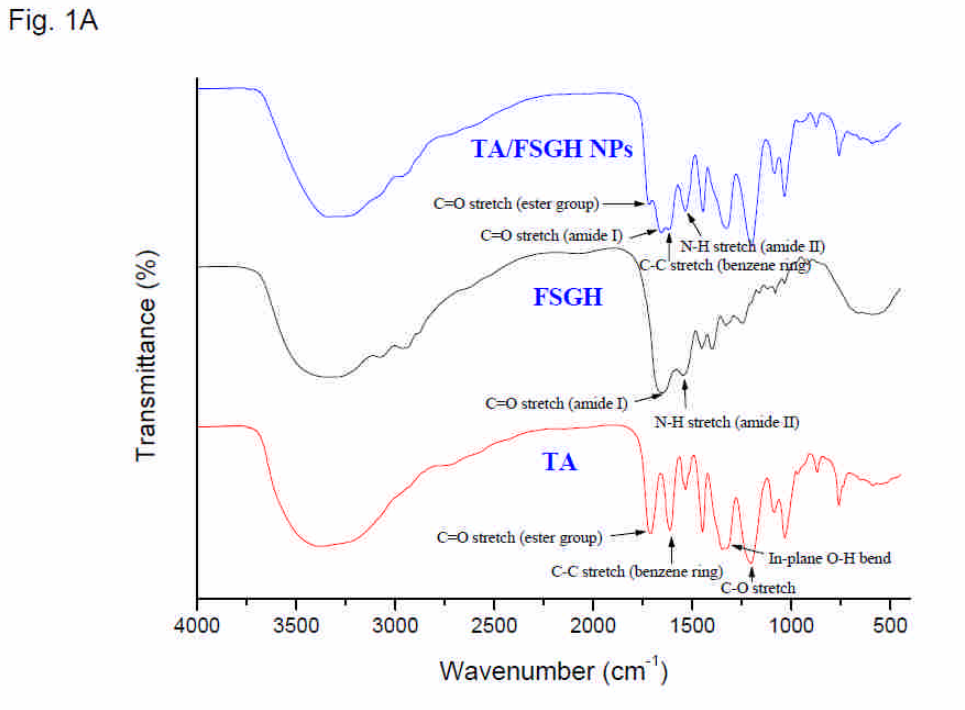

625

626

Fig. 1B

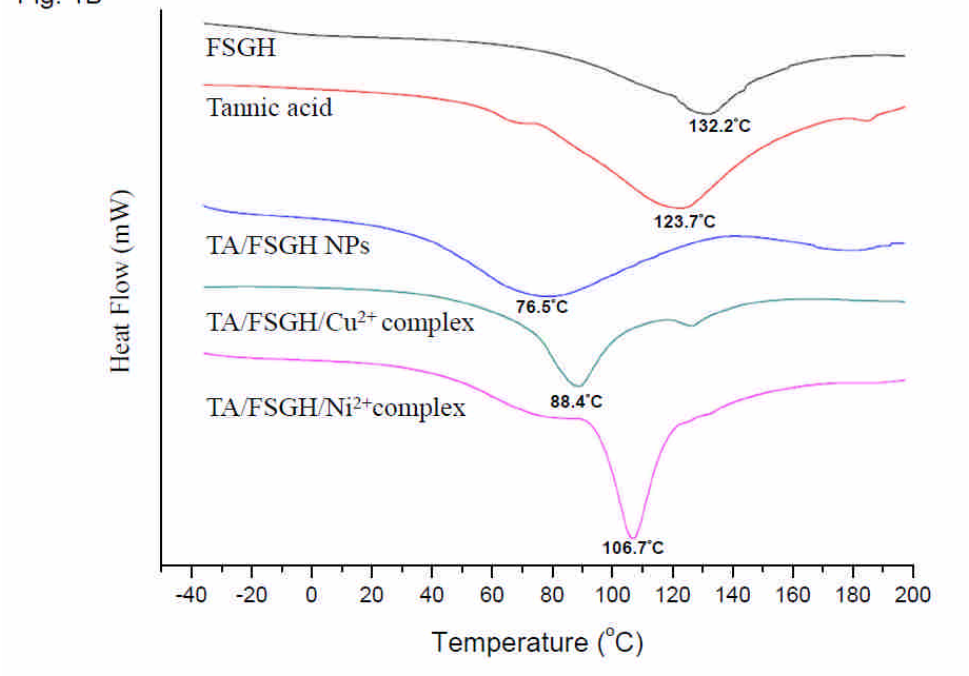

627

Fig. 1C

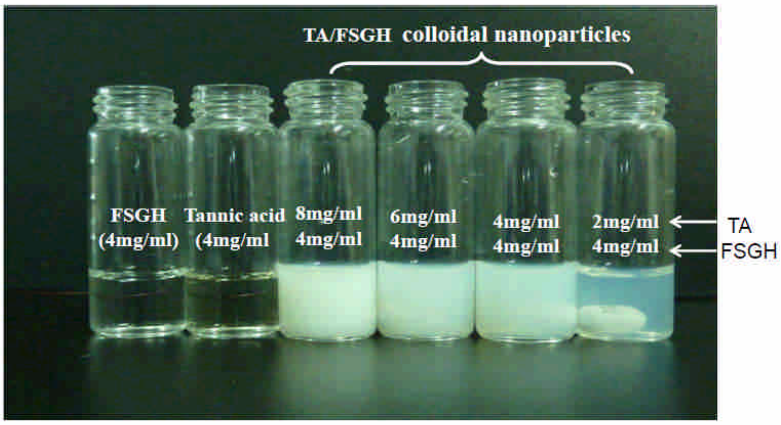

628

629

Fig. 1D

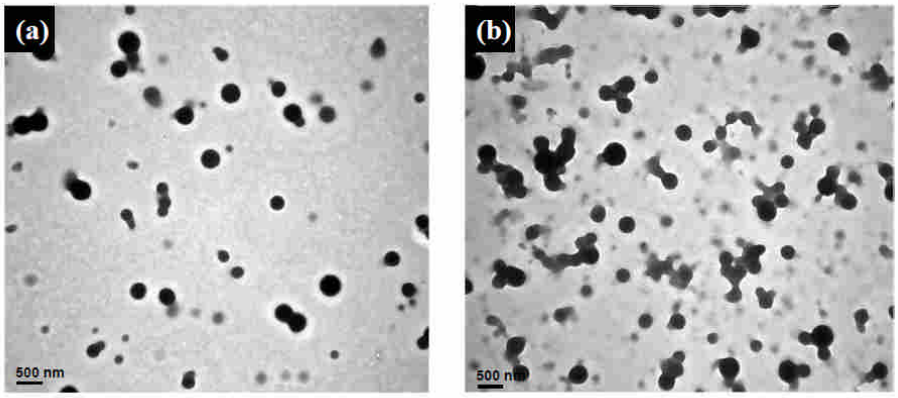

630

Fig. 2A

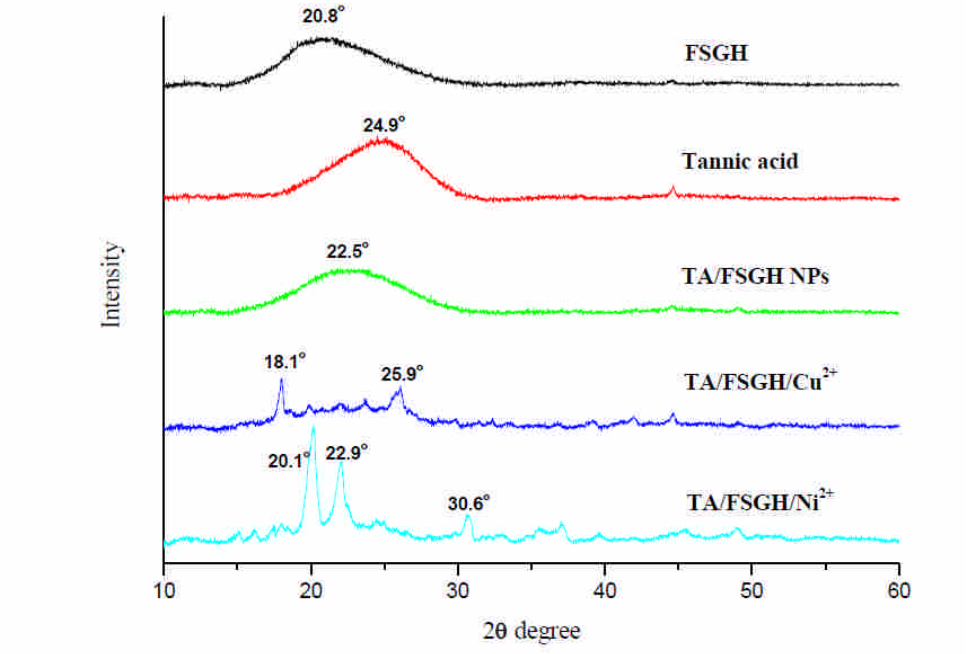

631

632

Fig. 2B

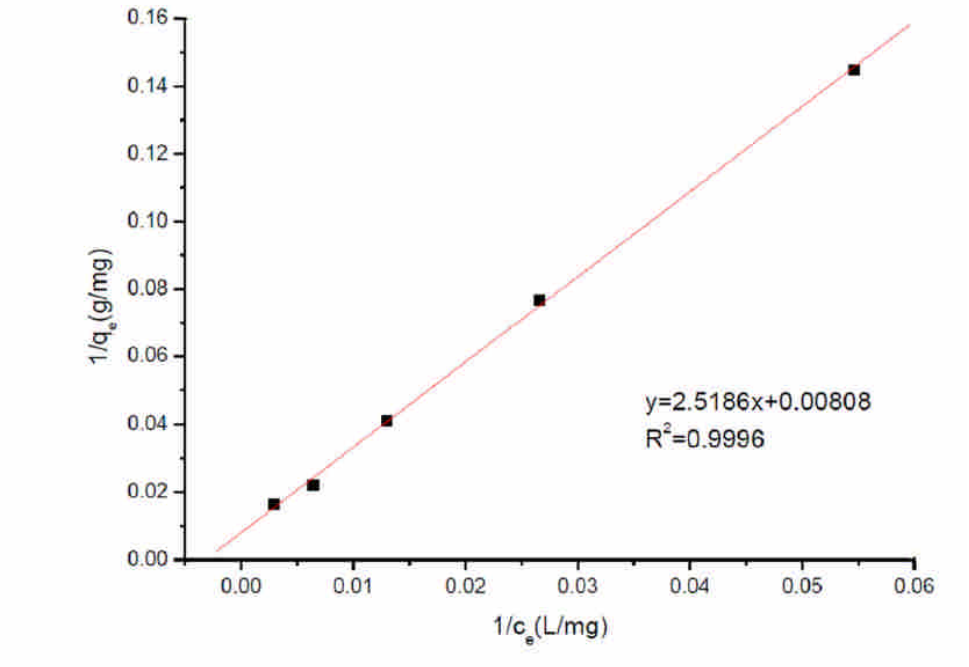

633

Fig. 2C

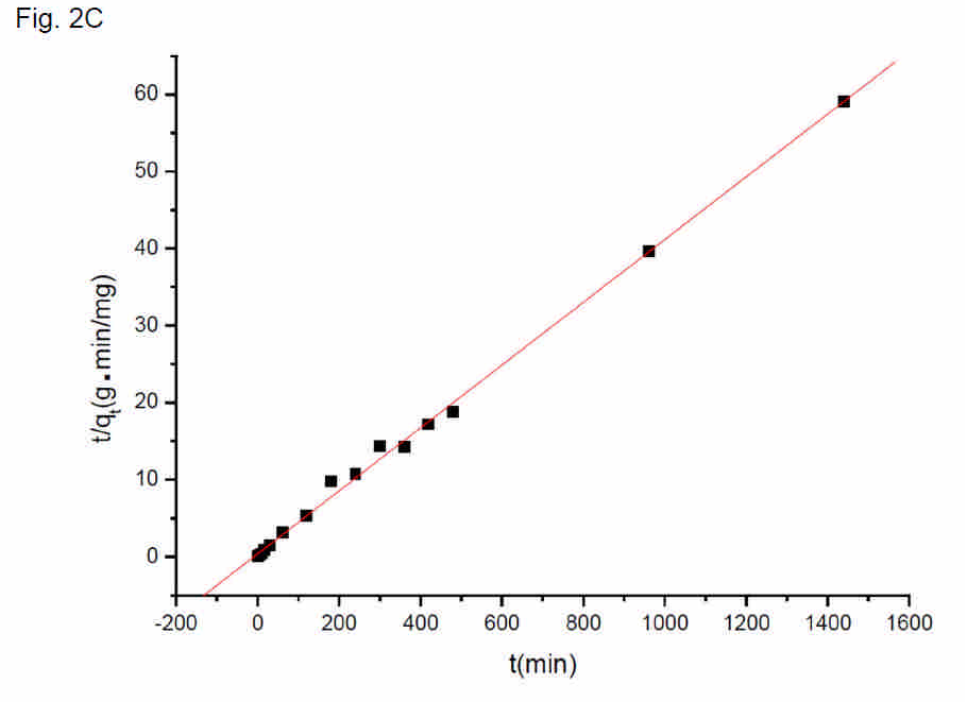

634

635

Fig. 2D

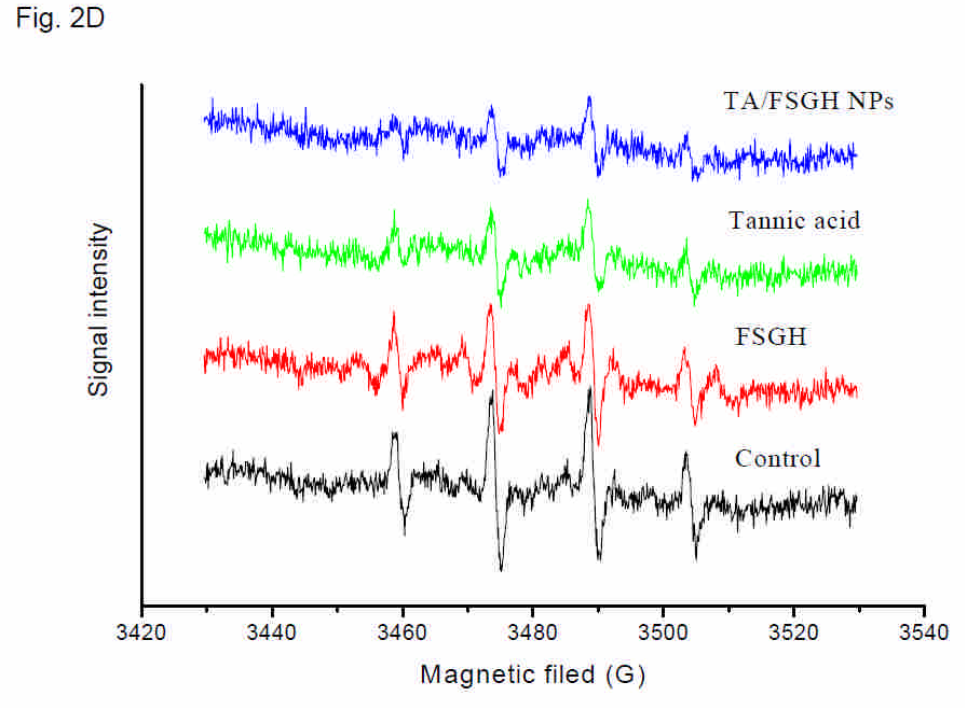

636

Fig. 3A

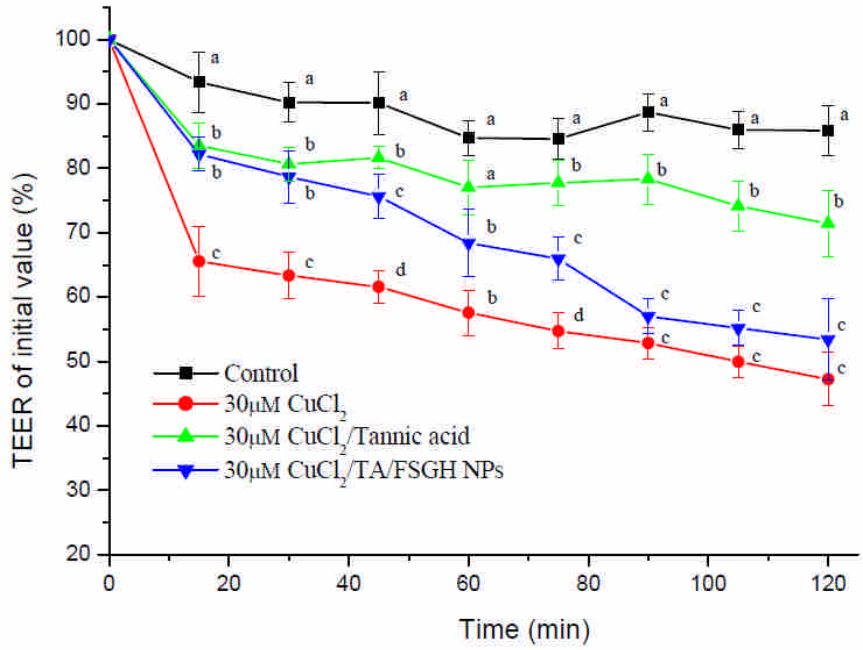

637

638

Fig. 3B

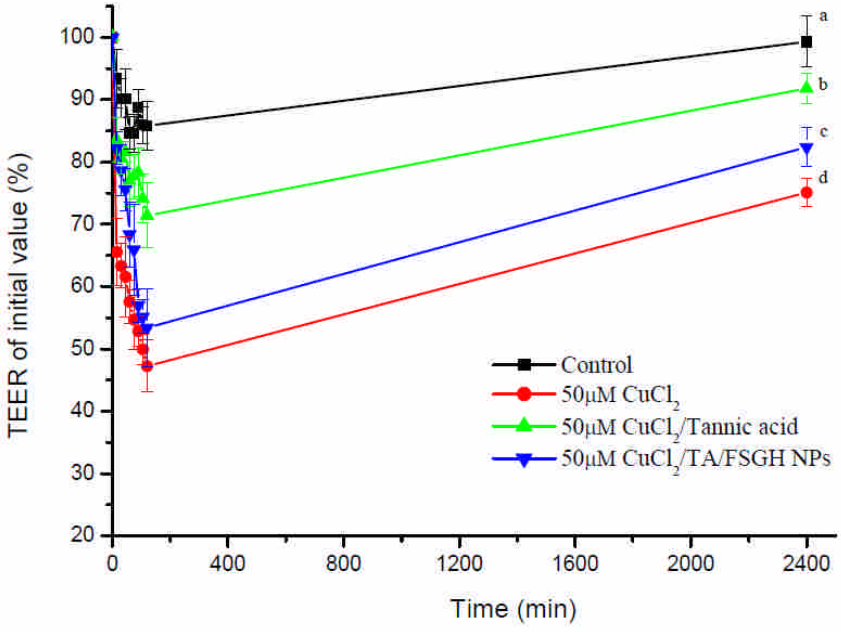

639

Fig. 3C

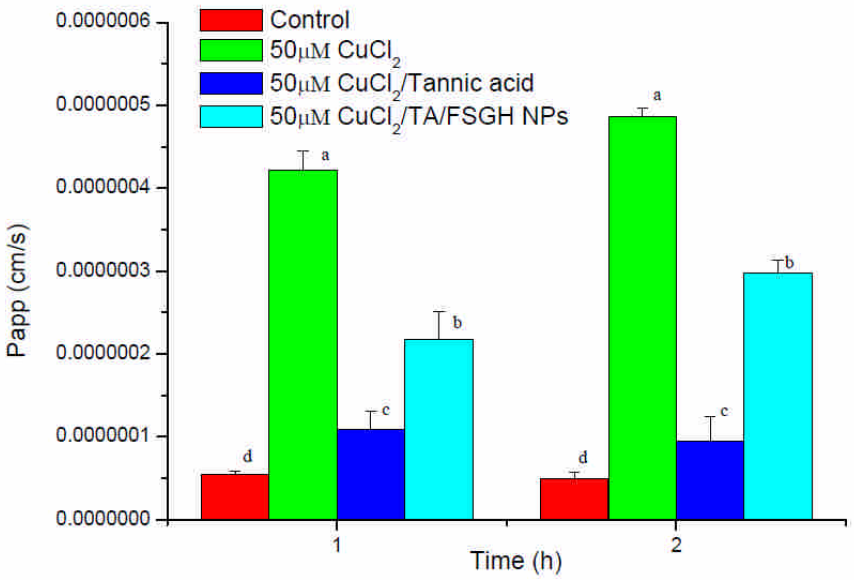

640

641

Fig. 3D

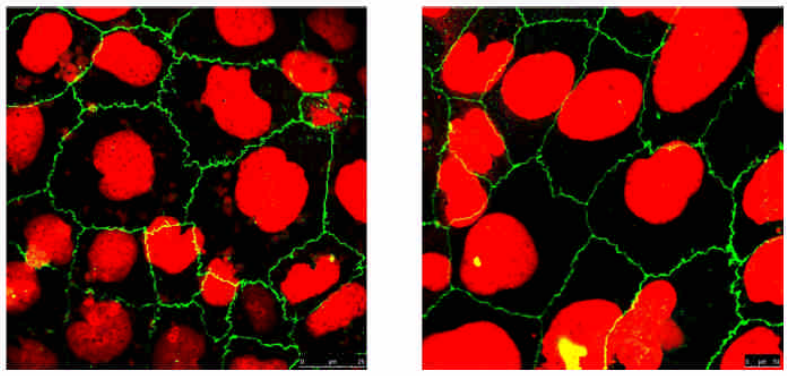

642

643

Fig. 4A

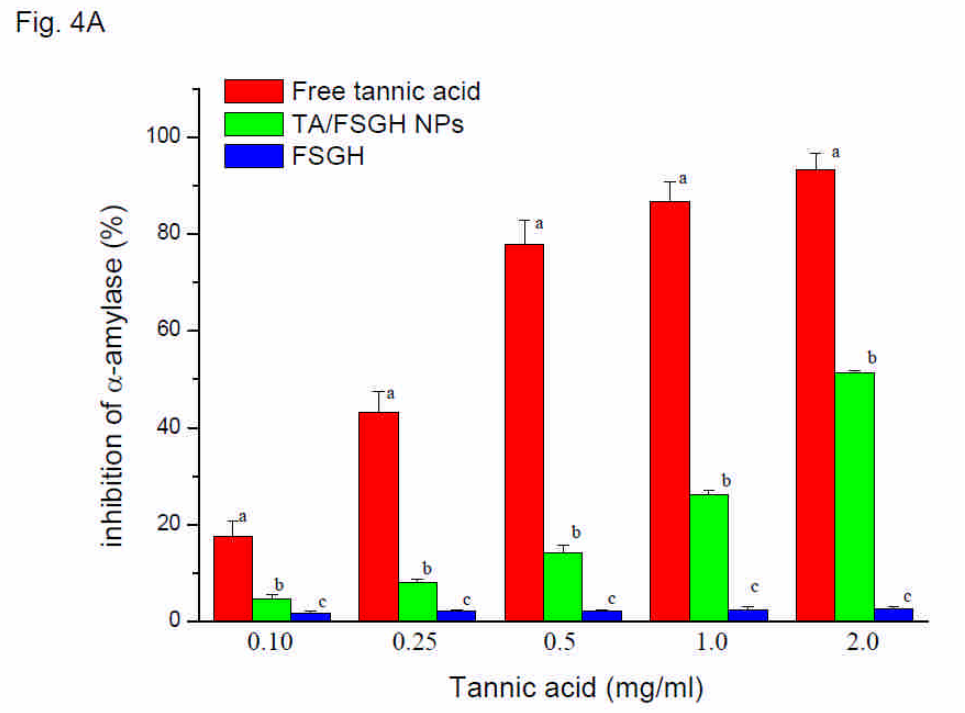

644

645

Fig. 4B

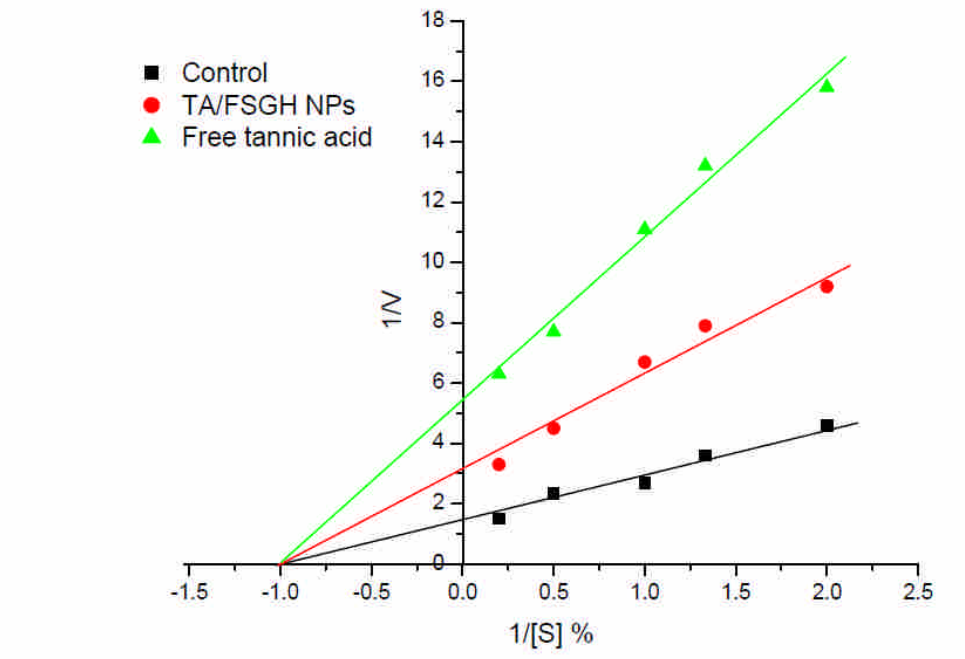

646